#4739

NUMERICAL STUDY OF FLOW AND CONTAMINANT DIFFUSION FIELDS AS AFFECTED BY FLOW OBSTACLES IN CONVENTIONAL-FLOW-TYPE CLEAN ROOM

S. Murakami, Dr.Eng.
Member ASHRAE

S. Kato, Dr.Eng.
Member ASHRAE

Y. Suyama
Member ASHRAE

ABSTRACT

An apparatus placed in a clean room has a great influence on the flow field. Such flow obstacles often generate airborne particles into the air flow. Thus, it is very important to clarify the flow field and contaminant diffusion field around flow obstacles.

In this paper, the airflow distribution and the contaminant diffusion field in a conventional-flow-type clean room with flow obstacles in various arrangements are analyzed by means of model experiments and three-dimensional numerical simulations. Correspondence between the simulations and the experiments is fairly good, both for the velocity field and for the contaminant diffusion field. On the basis of this validated procedure, further analyses of the airflow in a clean room with flow obstacles variously arranged are conducted by means of numerical simulations based on the k-ϵ turbulence model. From these analyses, much useful information is obtained concerning the velocity field and the contaminant diffusion field around obstacles and also concerning the influence of flow obstacles on the entire flow field.

INTRODUCTION

In many fields of industry, the conventional-flow-type clean room is now indispensable for use in quality control. An understanding of the flow field and the contaminant diffusion field is very important in designing effective contamination control for such rooms. In preceding papers (Murakami et al. 1987, 1988, 1989), the flow field and its resulting diffusion field of contaminant in conventional-flow-type clean rooms were analyzed with model experiments and numerical simulations based on the k-ϵ two-equation turbulence model.

In this paper, the effects of flow obstacles in a room on the flow field and the diffusion field are analyzed by numerical simulations. Since an apparatus in a clean room has a great influence on the flow field and often generates airborne particles, clarification of the flow and diffusion fields around flow obstacles is required. Numerical simulation of turbulent airflow allows us to precisely analyze the flow and diffusion field in a room. The accuracy of numerical simulation was well validated by Murakami (1987). In another study, it was shown that the flow and diffusion fields were mainly characterized by serial combinations of "flow units," each composed of an inflow and the rising streams around it (Murakami et al. 1988). It was also demonstrated that the arrangement of supply and exhaust openings has a great influence on the diffusion field (Murakami et al. 1989). This paper extends the previous studies to analyze the effects of flow obstacles on the flow and diffusion fields. The main contents are as follows:

1. The accuracy of numerical simulation of the flow and diffusion fields around obstacles is validated by comparison with the results of model experiments.
2. The structure of the flow and diffusion fields around flow obstacles in various arrangements is analyzed.
3. The effect of such flow obstacles on the entire flow field is analyzed.

MODELS OF CLEAN ROOM AND FLOW OBSTACLES

The clean room model used here has nine supply outlets and four exhaust inlets. It was called type 4 in preceding papers (Murakami et al. 1988, 1989). The configurations of this room model and the flow obstacles are shown in Figure 1. Table 1 lists the six cases analyzed here and illustrates the various arrangements of flow obstacles and various source positions of contaminant. These cases are:

1. Case 0: Standard type with no flow obstacle.
2. Cases 1-3: Arrangement with one box-type flow obstacle (1) in contact with the side wall, (2) under the supply jets, and (3) between the supply jets, respectively.
3. Case 4: Arrangement with a table-type flow obstacle in contact with the side wall.
4. Case 5: Arrangement with three box-type flow obstacles.

In this study, the contaminant is generated in three ways: one-point generation, uniform generation on a surface, and uniform generation throughout the room. The position of the source points (A, B, C, D, E) of the contaminant generation in each case is shown by circles in Table 1.

The contaminant in this study is assumed to be of passive scalar quantity and thus of no effect on the momentum equation. Therefore, not only the buoyancy effect but also its absorption at wall surfaces are assumed to be negligible if the contaminant is gaseous material. Furthermore, deposit, sedimentation, and cohesion are also assumed to be negligible if the contaminant is aerosol. Therefore, its transportation or diffusion is fully controlled by the airflow. The flow field and the resulting diffusion field are assumed to be in a steady state.

Shuzo Murakami is a Professor and **Shinsuke Kato** is an Associate Professor at the Institute of Industrial Science, University of Tokyo, Japan; **Yoshimi Suyama**, formerly Joint Researcher at the Institute of Industrial Science, University of Tokyo, is now Researcher for the Institute of Technology, Hazama-Gumi Co. Ltd., Japan.

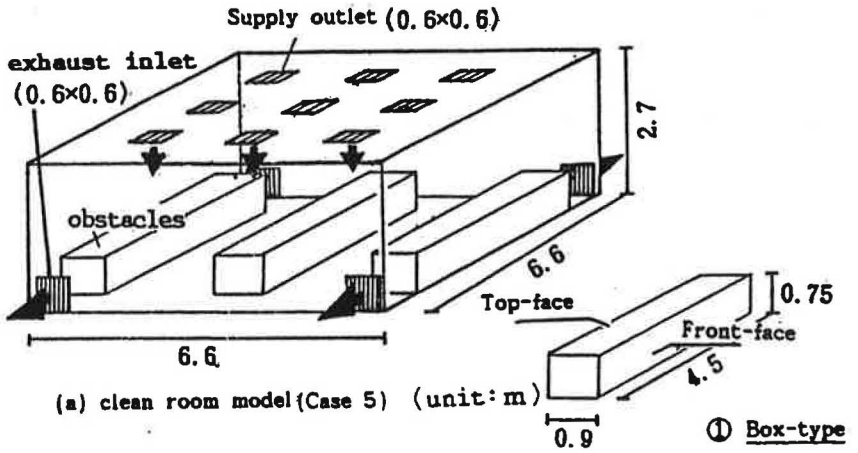

(b) **Specifications of room model**

- Dimensions of Plan : 6.6m×6.6m
- Height of Ceiling : 2.7m
- Number of Supply Outlets : 9
- Number of Exhaust inlets : 4
- Supply Air Velocity : 1.0 m/s
- Number of Air Changes : 99.2 N/h

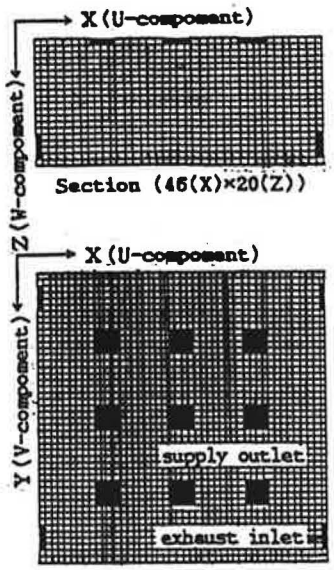

dimensions of a cell : 15cm×15cm×15cm

(d) Mesh dividing system

Figure 1 *Clean room model and flow obstacles*

TABLE 1
Specifications of Cases Analyzed

Cases	Case 0	Case 1	Case 2	Case 3	Case 4	Case 5
Flow Obstacles	No Obstacle	One Box-type Obstacle	One Box-type Obstacle	One Box-type Obstacle	One Table-type Obstacle	Three Box-type Obstacles
Arrangement of Flow Obstacles and Position of Contaminant Generation (shown by the circle in the section)	A B C D E (section) (plan)	(in contact with the wall)	(under suply jets)	(between supply jets)	(in contact with the wall)	(in contact with the walls and in center of the room)
Name of the Point of Contaminant Generation	A:adjacent to the wall B:under supply jet C:between obstacles D:between supply jets E:center of the room S:SVE3 (throughout the room)	A:adjacent to the wall (on the top-face of obstacle) E:center of the room S:SVE3	B:under supply jet E:center of the room S:SVE3	D:between supply jets E:center of the room S:SVE3	A:adjacent to the wall E:center of the room S:SVE3	A:adjacent to the wall C:between obstacles E:center of the room E':surface of top-face C':surface of floor between obstacles S:SVE3

remarks 1 Numerical simulations were conducted for all cases.
2 Model experiment was conducted only for case 1.

The contaminant generation rate is also assumed to be constant.

In this study, physical quantities are made dimensionless by dividing by representative quantities. These quantities are the width of the supply opening, L_0, its mean velocity, U_0, and the mean contaminant concentration at the exhaust inlet, C_0.

MODEL EXPERIMENT

Model experiments were conducted using a one-sixth scale model (Murakami et al. 1987, 1988).

Air velocity was measured by means of a tandem-type, parallel hot-wire anemometer, which can discern the vector components of turbulent flow (Murakami et al. 1980).

The distribution of contaminant concentration was investigated by means of a tracer gas diffusion experiment (Murakami et al. 1988). Since ethene (C_2H_4), whose density is nearly the same as that of air, was used as the tracer, the buoyancy effect of the tracer can be disregarded. Its concentration was measured by means of F.I.D. gas chromatography.

NUMERICAL SIMULATION

Model equations (k - ϵ two-equation turbulence model [Launder et al. 1974]) are given in Table 2. These equations are discretized by a control volume method (almost the same as a finite difference method), and the steady-state solution is obtained by a time-marching method. The simultaneous pressure

TABLE 2
k - ϵ Two-Equation Model (3-D)

$\frac{\partial U_i}{\partial X_i} = 0$	(1) Continuity equation
$\frac{\partial U_i}{\partial t} + \frac{\partial U_i U_j}{\partial X_j} = -\frac{\partial}{\partial X_i}\left(\frac{P}{\rho} + \frac{2}{3}k\right) + \frac{\partial}{\partial X_j}\left(\nu_t\left(\frac{\partial U_i}{\partial X_j} + \frac{\partial U_j}{\partial X_i}\right)\right)$	(2) Momentum equation
$\frac{\partial k}{\partial t} + \frac{\partial k U_j}{\partial X_j} = \frac{\partial}{\partial X_j}\left(\frac{\nu_t}{\sigma_1}\frac{\partial k}{\partial X_j}\right) + \nu_t S - \varepsilon$	(3) Transport equation for k
$\frac{\partial \varepsilon}{\partial t} + \frac{\partial \varepsilon U_j}{\partial X_j} = \frac{\partial}{\partial X_j}\left(\frac{\nu_t}{\sigma_2}\frac{\partial \varepsilon}{\partial X_j}\right) + C_1\frac{\varepsilon}{k}\nu_t S - C_2\frac{\varepsilon^2}{k}$	(4) Transport equation for ε
$\nu_t = k^{1/2} l = \left(C_\mu \frac{k^2}{\varepsilon}\right)$	(5) Equation for deciding ν_t
$\frac{\partial C}{\partial t} + \frac{\partial C U_j}{\partial X_j} = \frac{\partial}{\partial X_j}\left(\frac{\nu_t}{\sigma_3}\frac{\partial C}{\partial X_j}\right)$	(6) Concentration equation

here $S = \left(\frac{\partial U_i}{\partial X_j} + \frac{\partial U_j}{\partial X_i}\right)\frac{\partial U_i}{\partial X_j}$, $\sigma_1 = 1.0$, $\sigma_2 = 1.3$, $\sigma_3 = 1.0$, $C_\mu = 0.09$, $C_1 = 1.44$, $C_2 = 1.92$

TABLE 3
Boundary Conditions for Numerical Simulation

(1) Supply Outlet boundary: $U_t = 0.0$, $U_n = U_{out}$, $k = 0.005$, $l = 0.33$, $C = 0.0$
suffix t: tangential component, n: normal component
U_{out}: Supply outlet velocity, $U_{out} = 1.0$

(2) Exhaust Inlet boundary: $U_t = 0.0$, $U_n = U_{in}$, $\partial k/\partial Z = 0.0$, $\partial \varepsilon/\partial Z = 0.0$, $\partial C/\partial Z = 0.0$
U_{in}: Exhaust inlet velocity, $U_{in} = 2.25$

(3) Wall boundary: $\partial U/\partial Z_{z=0} = m U_{t\,z=h}/h$, $U_n = 0.0$, $\partial k/\partial Z = 0.0$, $\partial C/\partial Z = 0.0$

ε term in k equation:

$$\varepsilon_{z=h} = [C_\mu k_{z=h}^{3/2}]/[C_\mu^{1/4}\kappa h] \cdot \ln(E h (C_\mu^{1/2} k)^{1/2}/\nu)$$

ε equation:

$$\varepsilon_{z=h} = [C_\mu k_{z=h}^{3/2}]/[C_\mu^{1/4}\kappa h]$$

h: Length from the wall surface to the center of the adjacent cell
m: 1/7, Power law of profile $U_t \propto Z^m$ is assumed here.
E: 9.0, a function of the wall roughness (for a smooth wall)
ν: 1/Re, Kinematic viscosity
κ: 0.4, von Karman constant

(4) Finite difference Scheme: Time marching: Adams Bashforth Scheme (second order)
Convective terms of Ui, k, ε, and C: Quick Scheme (second order)

*1 Values are made dimentionless by Lo and Uo. and Co.
*2 Boundary condition for ε is changed a little from a previous study (Murakami et al. 1989).

velocity relaxation method is adopted for solving mean momentum equations following Viecelli (1967). Details are given in Murakami et al. (1987). The boundary conditions and schemes for the finite difference are shown in Table 3. The computational domain is discretized by sufficiently fine uniform grids (Figure 1d). One grid size is 0.25 (dimensionless), which corresponds to 1/44 of the room length, 1/18 of the ceiling height, and 1/5 of the height of the obstacle.

CORRESPONDENCE BETWEEN MODEL EXPERIMENT AND NUMERICAL SIMULATION

The experimental and numerical results for case 1 (arranging one box-type obstacle in contact with the side wall) are shown in Figures 2, 3, and 4. The velocity field is compared in Figures 2a and 3a. The airflow pattern of the simulation is very similar to that of the experiment, not only in the open area on the right side, but also in the recirculating region on the left side above the obstacle. The deviations of simulated values from the observed ones remain below 5%, which are normalized by the inflow velocity, for almost the whole room space.

The contaminant diffusion field is compared in Figures 2b and 4a. The contaminant diffuses into the left third of the room. A high concentration area appears above the obstacle, which becomes lower in the area near the ceiling. These characteristic patterns are rather well reproduced in the numerical simulation, although some discrepancy exists between the

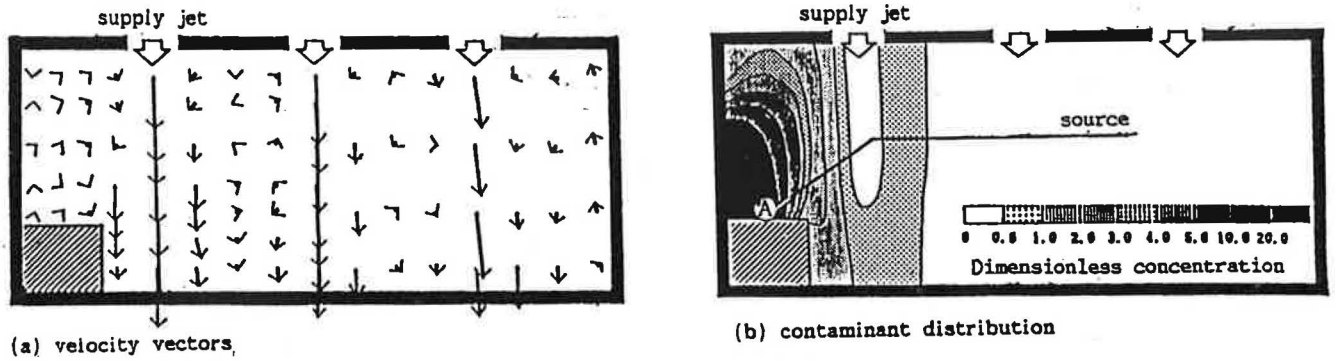

(Case 1: A box-type obstacle is placed in contact with the wall)

Figure 2 *Velocity vectors and contaminant distribution in Case 1 given by model experiment*

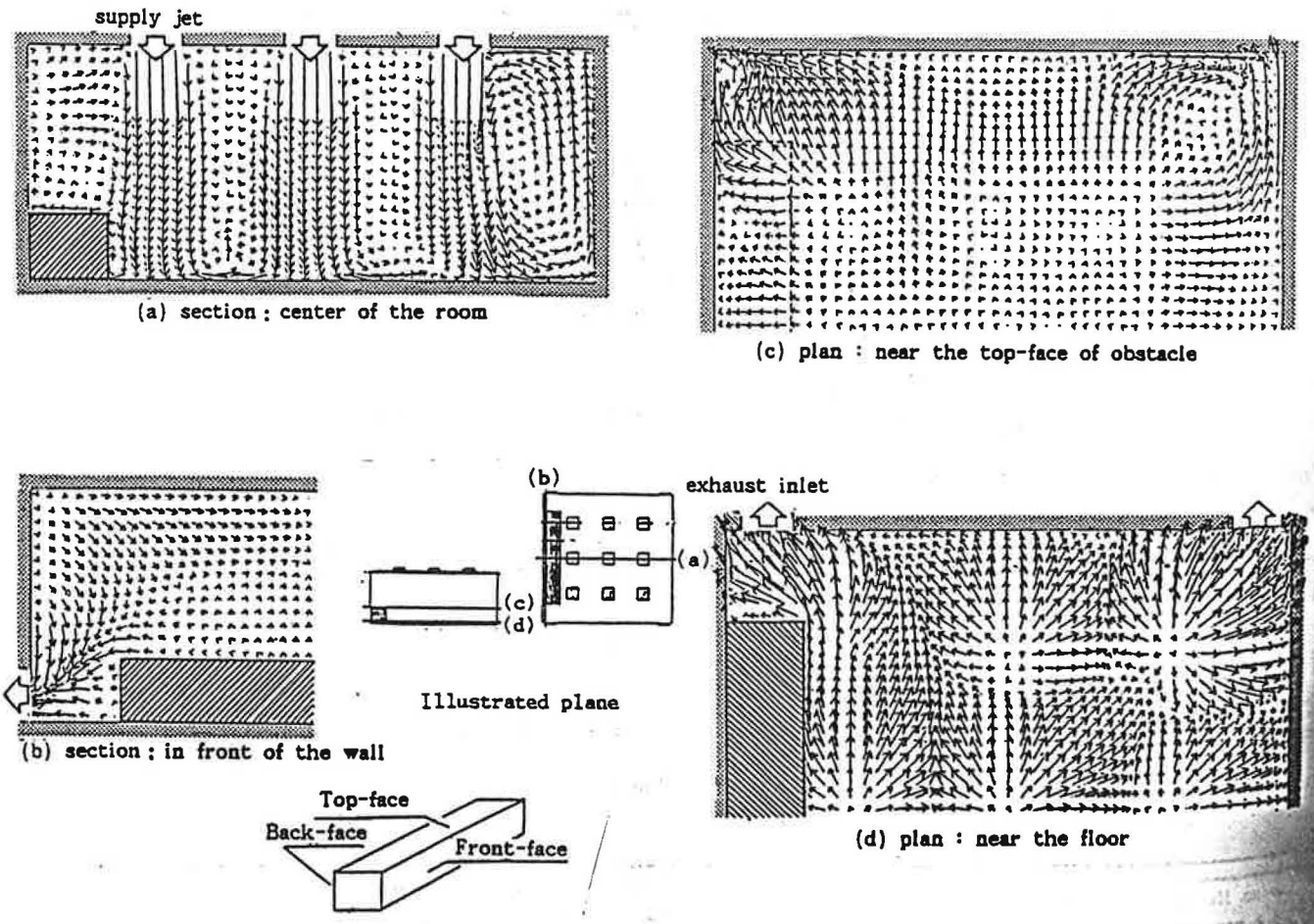

Figure 3 *Velocity vectors in Case 1 given by numerical simulation*

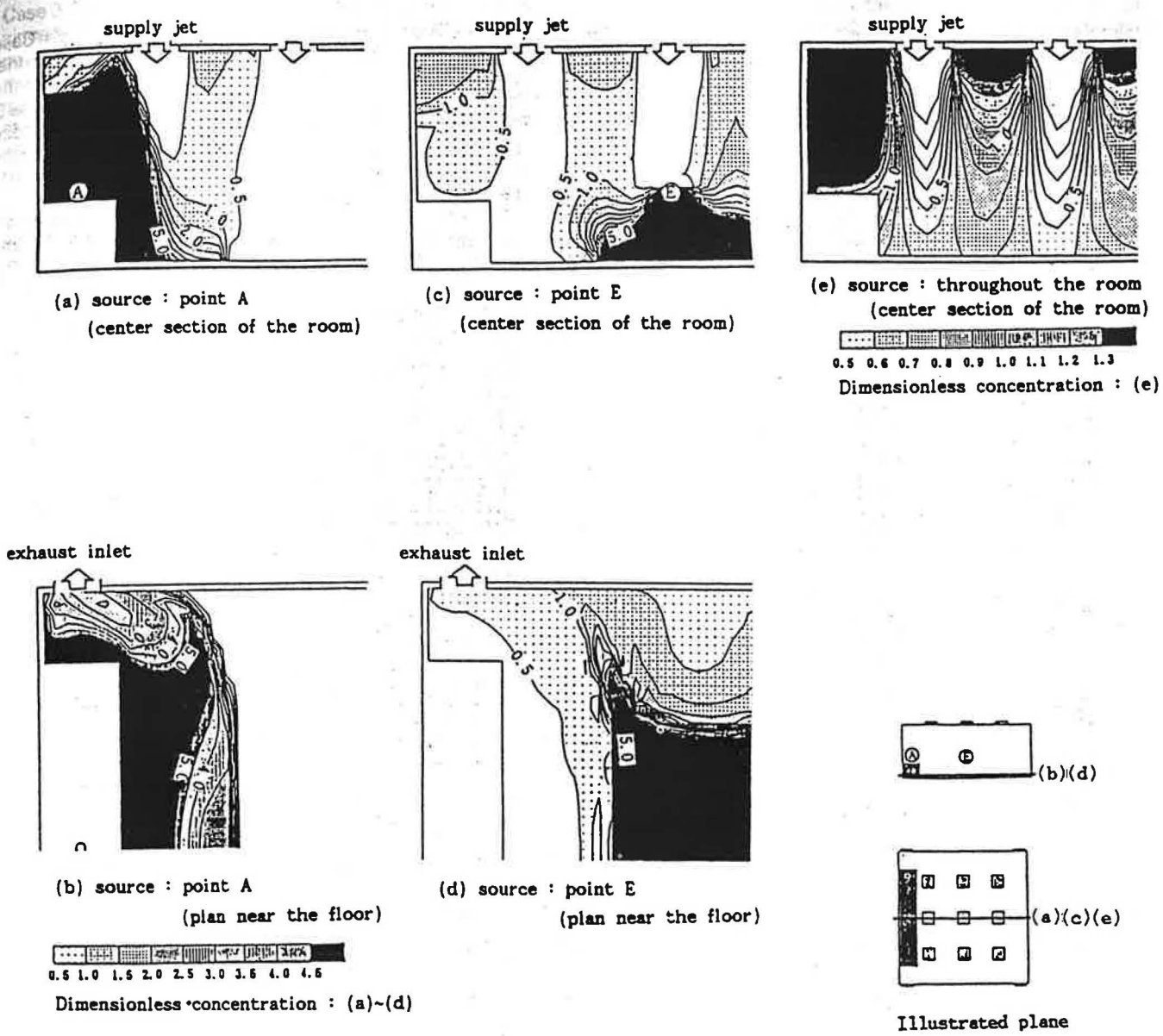

Figure 4 *Contaminant distributions in Case 1 given by numerical simulation*

experiment and the simulation in the area in front of the obstacle. The contaminant concentration deviation, from observed values ranges below 10% to 20% for almost the whole space; here the deviation is normalized by the averaged concentration of the exhaust air.

EXPRESSION OF CONTAMINANT DIFFUSION FIELD AND DEFINITION OF SVE1, 2, 3

In this study, the characteristics of contaminant diffusion fields are expressed by four methods:

1. Distribution of contaminant concentration by point source: this distribution is the most basic and allows intuitive comprehension of the contaminant diffusion field in a clean room.

2. SVE1 (the first Scale of Ventilation Efficiency): spatial average concentration. This value is proportional to the average time the contaminant is present in the room and indicates how quickly the contaminant generated in the room is exhausted by the flow field.

3. SVE2 (the second Scale of Ventilation Efficiency): mean radius of diffusion. This value represents the average spatial diffusion.

4. SVE3 (the third Scale of Ventilation Efficiency): concentration in the case of uniform contaminant generation throughout the room. At a given point, this value is proportional to the mean traveling time of supply air to that point. A high value for this concentration indicates a strong possibility of air contamination because the air mass must have traveled a long way from the supply outlet.

The details of these scales are described by Kato et al. (1988). The values of concentration are made dimensionless by dividing by the mean concentration at four exhaust openings, C_0. This mean value is the same for all cases in this paper. This type of dimensionless concentration was termed Model 1 in a previous study (Murakami et al. 1989).

INFLUENCE OF LOCATION OF SINGLE FLOW OBSTACLE (Cases 1, 2, 3)

Arranging a Box-Type Obstacle in Contact with the Side Wall (Case 1)

The velocity field and the contaminant diffusion field with a flow obstacle in contact with the side wall, as given by numerical

simulation, are shown in Figures 3 and 4. The standard case with no flow obstacle (Case 0) is also shown in Figures 5 and 6 as a reference. The designated names for each face of the obstacle used here are also illustrated in Figure 3.

Velocity Field The flow pattern in front of the side wall is illustrated in Figure 3b. As shown in Figure 3a, a recirculating flow appears above the obstacle and part of it flows into the supply jet near the ceiling. The air above the top face of the obstacle moves toward the side wall, as shown in Figures 3a and 3c. In front of the obstacle, the air moves toward the exhaust opening along the front face of the obstacle, as shown in Figure 3d.

The airflow pattern near the side wall with no obstacle (Case 0) is also shown in Figures 5a and 5b. It differs greatly from that of Case 1. In the open area on the right side far from the obstacle, there is little difference between Case 1 and Case 0. The effect of the flow obstacle is confined within the space around the obstacle, namely, within the "flow unit" in which the obstacle exists. The concept of "flow unit" is described in detail in a previous paper (Murakami et al. 1988).

Contaminant Concentration Field When the contaminant is generated on the top face of the obstacle (Point A, Figures 4a and 4b), the contaminant diffuses into the left third of the

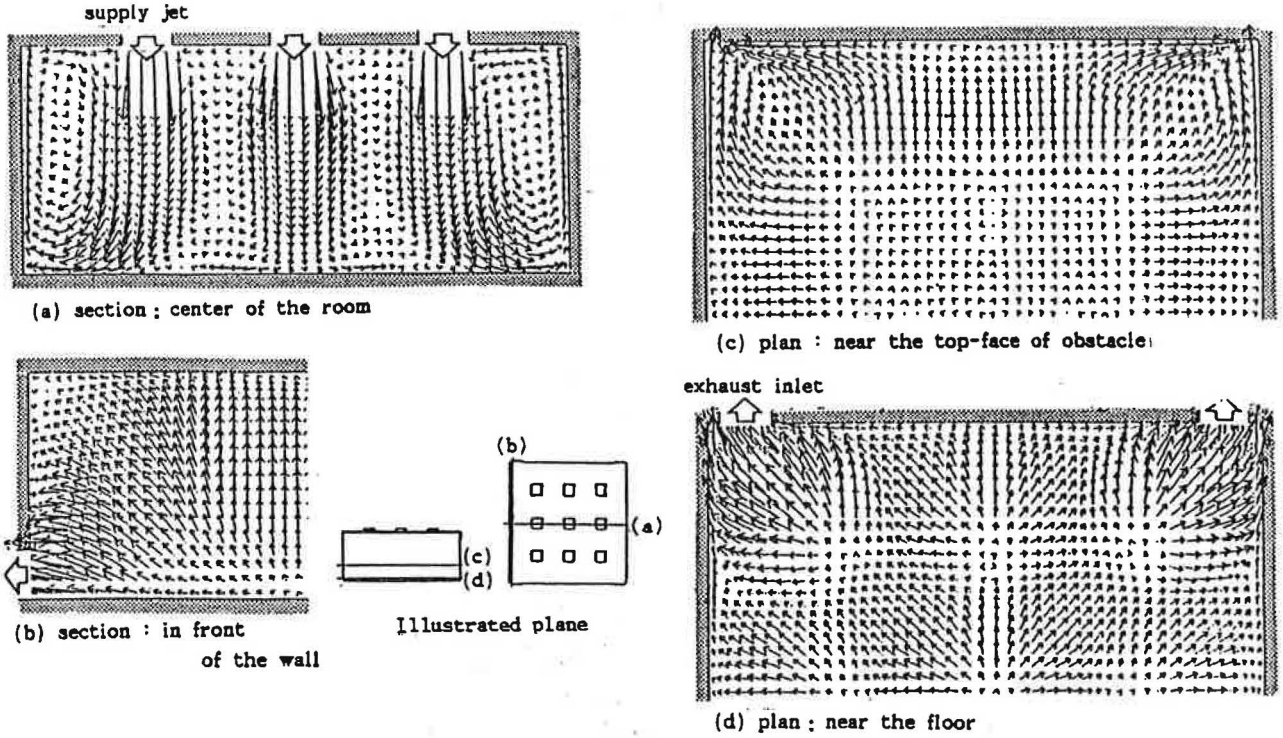

Figure 5 *Velocity vectors in Case 0 (No Obstacle, cf. Murakami et al. 1989)*

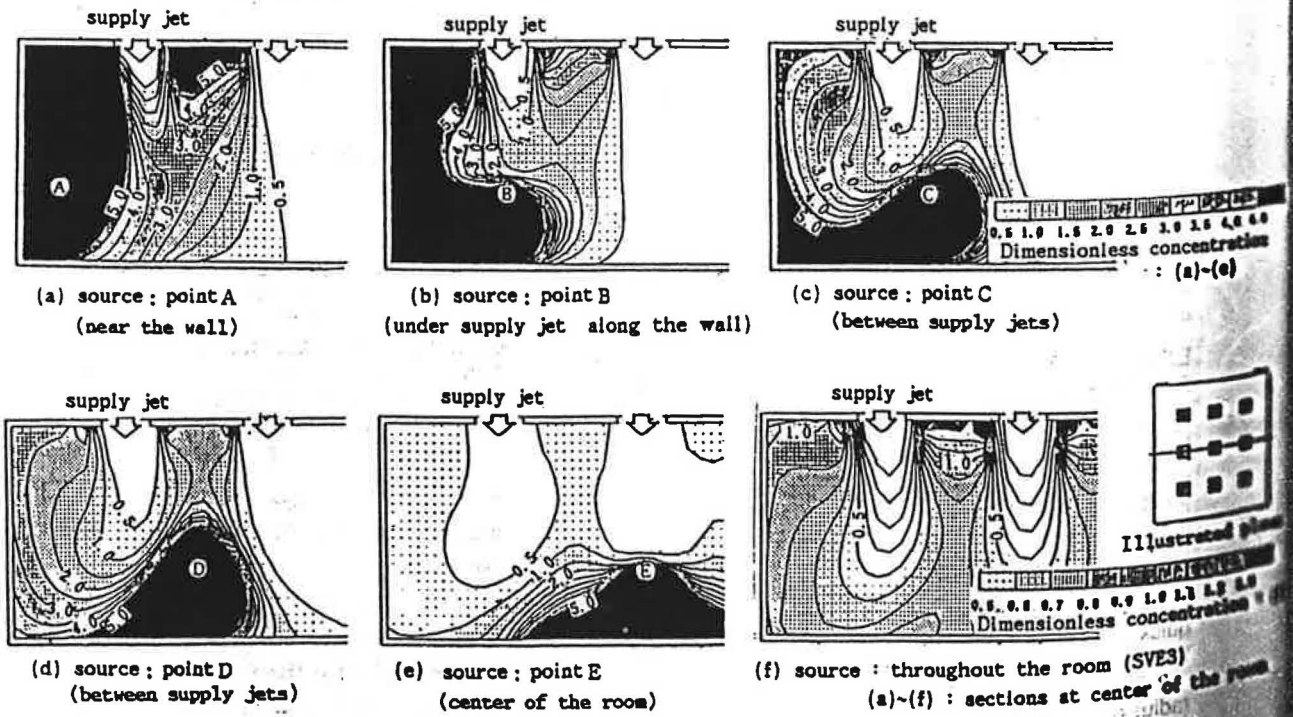

Figure 6 *Contaminant distributions in Case 0*

room. This one-third diffusion pattern is similar to the result in Case 0. The concentration near the ceiling becomes rather low, since the clean air is convected along the ceiling from the corner area. The value of SVE1 is 2.1 (dimensionless), which is much larger than its value in Case 0 (1.7). The value of SVE2 is 2.5 (dimensionless), smaller than in Case 0 (3.1). The values of SVE1 and SVE2 for all cases are tabulated in Table 4.

When the contaminant is generated in the center of the room (Point E, Figures 4c and 4d), it spreads throughout the whole room. But the space around the obstacle is not contaminated because air from the three supply jets near the side wall flows into this area. The value of SVE1 is 1.6 and, hence, larger than in Case 0 (1.4). Thus the ventilation efficiency for exhausting the contaminant decreased to some degree in Case 1. The value of SVE2 in Case 1 is 4.3, almost the same as in Case 0 (4.2). Although the obstacle beside the wall has almost no effect on the velocity field around point E, the diffusion field for contaminant generation at Point E is influenced whether the flow obstacle is present or not.

The value of SVE3 is compared in Figures 4e and 6f. The concentration above the obstacle in Case 1 is much higher than in Case 0, thereby indicating that supplied clean air requires a long traveling time to reach this recirculating area around the obstacle.

Arranging a Box-Type Obstacle under Supply Jets (Case 2)

The velocity and diffusion fields when a flow obstacle is placed under the supply jets are shown in Figures 7 and 8.

TABLE 4
Values of SVE1 and SVE2

sources / Case No.	near the wall (point A)	under supply jet (point B)	between obstacles (point C)	between supply jets (point D)	center of the room (point E)
Case 0	1.7 *1 3.1 *2	1.3 3.2	1.4 3.4	1.5 3.6	1.4 4.2
Case 1	2.1 2.5	—	—	—	1.6 4.3
Case 2	—	1.9 3.7	—	—	1.6 4.2
Case 3	—	—	—	1.7 3.2	1.5 4.0
Case 4	1.4 2.5	—	—	—	1.3 4.2
Case 5	2.6 3.0	—	1.5 4.0	—	2.0 4.3

*1 upper line of the space : SVE1 (non-dimensionalized by Co)
*2 lower line of the space : SVE2 (non-dimensionalized by Lo)

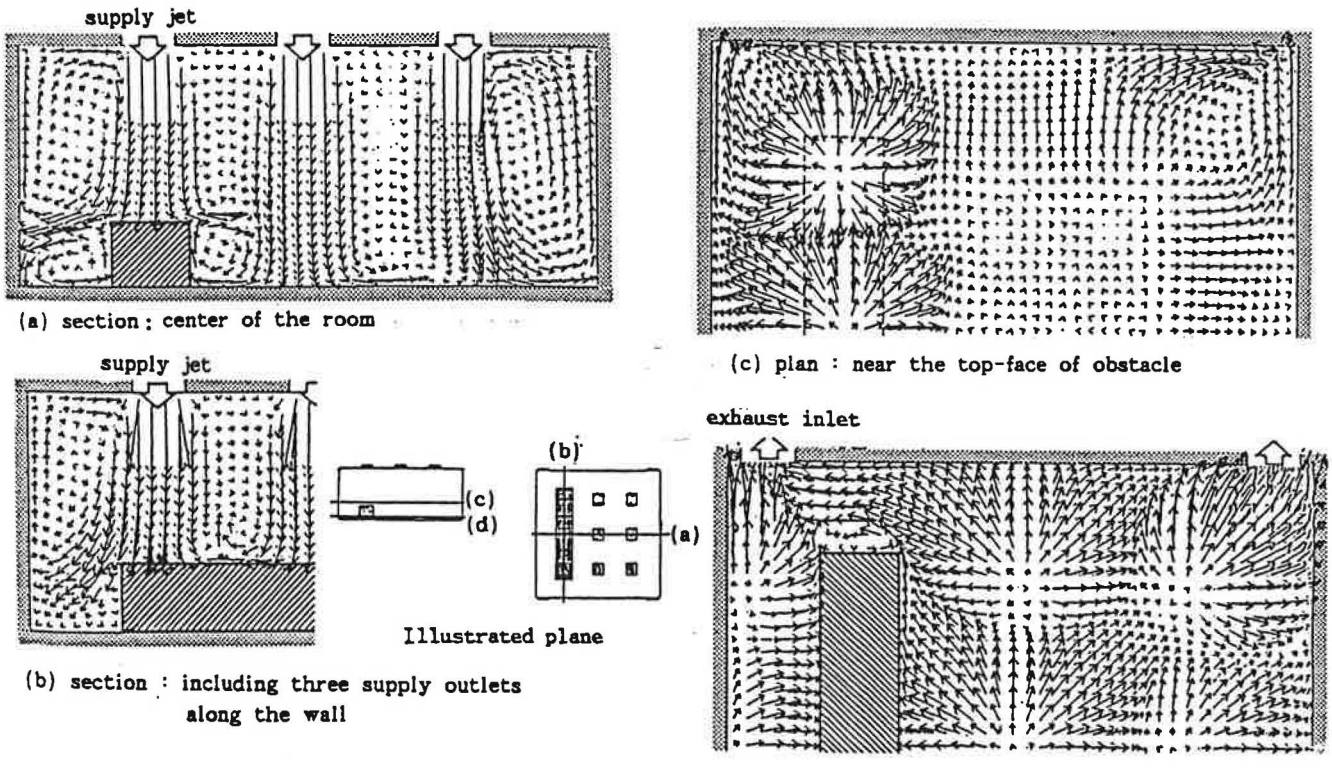

(Case 2 : A box-type obstacle is placed under supply jets)

Figure 7 *Velocity vectors in Case 2*

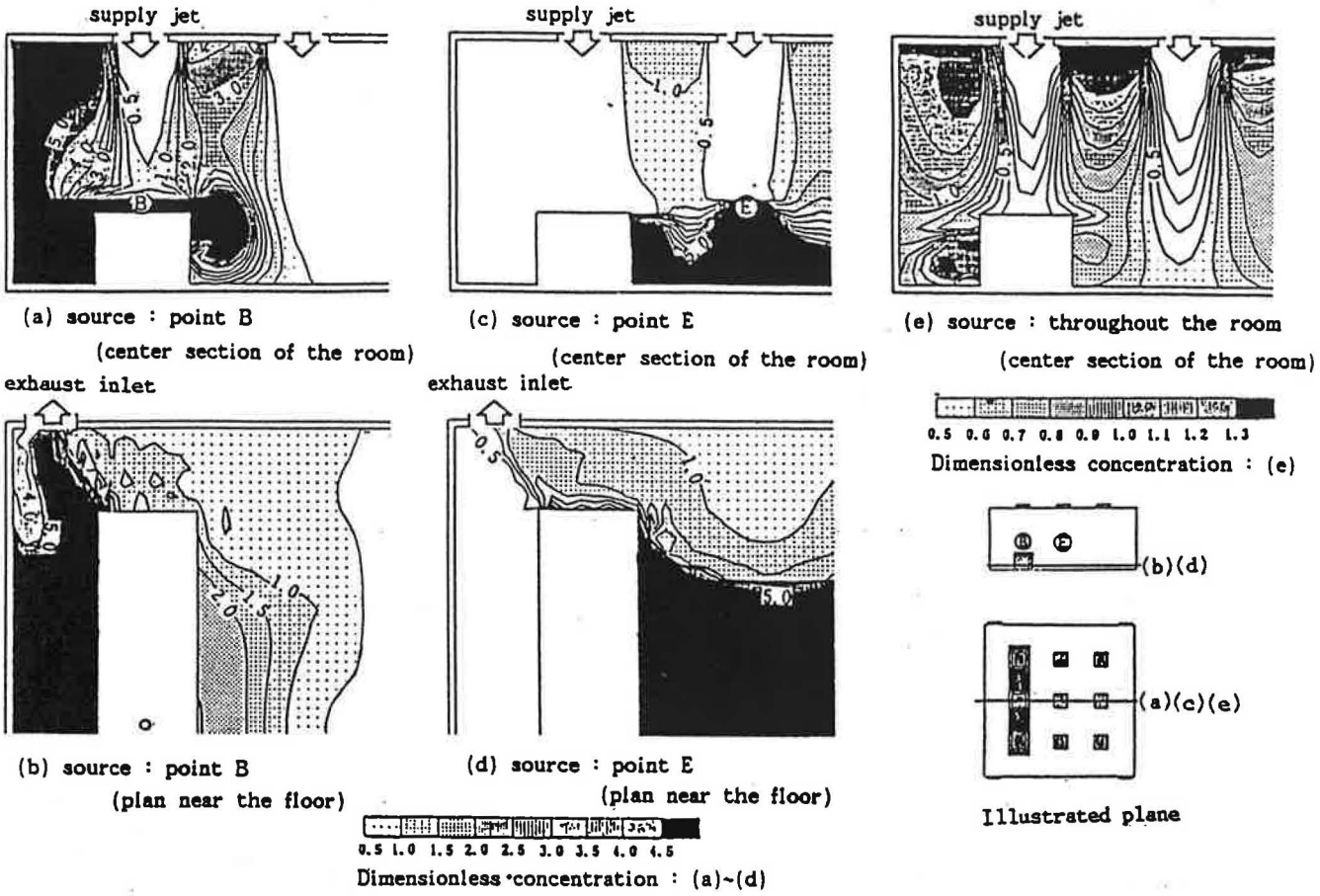

Figure 8 *Contaminant distributions in Case 2*

Velocity Field The supply jet attacks the top face of the obstacle and diverges in all directions (Figures 7a and 7c). A small rising stream appears above the top face between the supply jets (Figure 7b). Recirculating flows exist in front of the back and front faces of the obstacle (Figure 7a). In the open area on the right, the velocity field of Case 2 is the same as that of Case 0; hence, the effect of this arrangement of the flow obstacle is confined within a rather small area near the obstacle.

Contaminant Diffusion Field When the contaminant is generated at the top face of the obstacle (Point B), it is convected horizontally by the diverging flow at this area (Figure 8a). The high concentration spreads into the recirculating region along the side wall and also into the area in front of the back and front faces (Figure 8a). The contaminated area occupies the left half of the room (Figures 8a and 8b). The value of SVE1 in Case 2 is 1.9, much larger than in Case 0 (1.3). The value of SVE2 in Case 2 is 3.7, also larger than in Case 0 (3.2).

When the contaminant is generated at the center of the room (Point E), it spreads into the open area on the right where no obstacle is arranged (Figures 8c and 8d). The space to the left of the obstacle is clean, since the spread of the contaminant is blocked by the obstacle. The value of SVE1 is 1.6, larger than in Case 0 (1.4). The value of SVE2 is 4.2, which is the same as in Case 0.

The value of SVE3 is very low above the top face of the obstacle because of the direct supply of clean air (Figure 8e). This indicates that the placement of an apparatus whose top face must be extremely clean should be selected carefully and with the properties of the diffusion field in mind in order to take advantage of the flow structure of conventional-flow-type clean rooms.

Arranging a Box-Type Obstacle between Supply Jets (Case 3)

The flow and diffusion fields for Case 3 are illustrated in Figures 9 and 10, where a box-type obstacle is arranged between the supply jets.

Velocity Field The velocity field at the top face of the obstacle is horizontal and flows mainly toward the exhaust opening, as shown in Figures 9a and 9c. Rising streams appear at some point above the obstacle (Figure 9b). The supply jets at the center attack the floor and thus diverge toward the open area on the right because of blocking on the left side by the obstacle. The flow pattern in the open area on the right side is similar to that in Case 0 where no obstacle is arranged.

Contaminant Diffusion Field When the contaminant is generated on the top face of the obstacle (Point D, Figure 10a), it stays around the obstacle, since the diffusion field is blocked by the rows of supply jets on both sides (Figure 10a). The contaminated area is the left half of the room (Figures 10a and 10b). The value of SVE1 is 1.7, which is higher than in Case 0 (1.5). The value of SVE2, on the other hand, is 3.2, significantly smaller than in Case 0 (3.6).

When the contaminant is generated at the center of the room (Point E), it diffuses into the right half of the room, since diffusion toward the left is blocked by the obstacle (Figures 10c and 10d). The top face of the obstacle is clean since the supply jet attacks it. The value of SVE1 is 1.5, a little larger than in Case 0 (1.4). The value of SVE2 (4.0), on the other hand, is smaller than in Case 0 (4.2). The distribution of SVE3 (Figure 10e) is similar to that in Case 0.

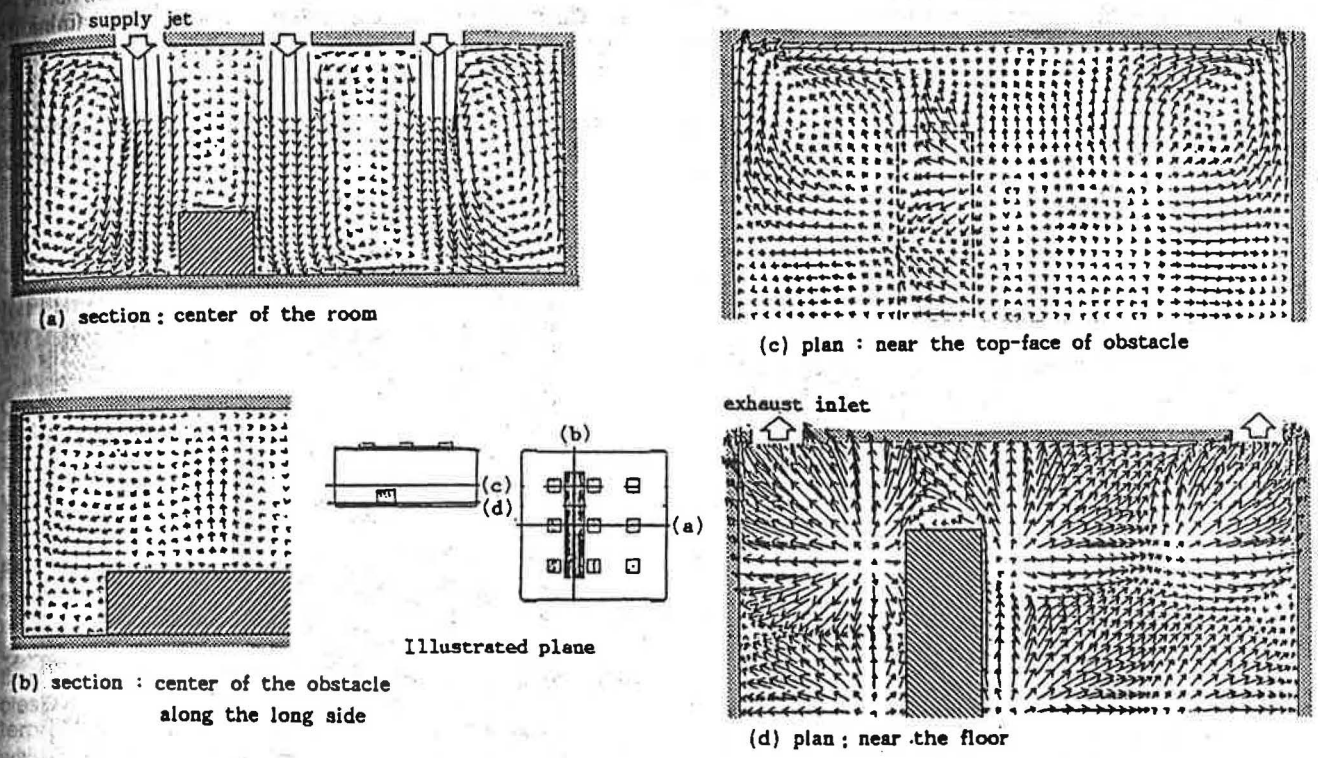

(Case 3 : A box-type obstacle is placed between supply jets)

Figure 9 *Velocity vectors in Case 3*

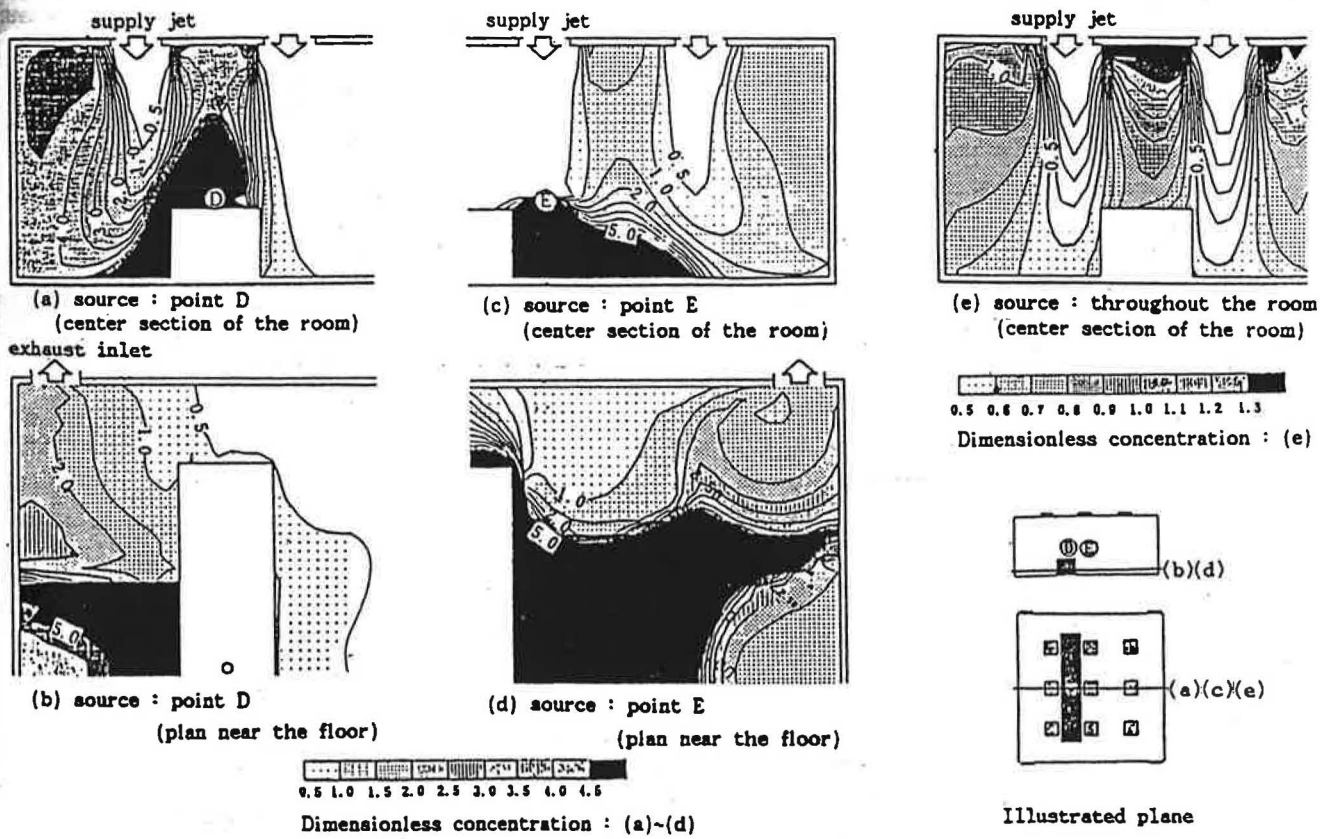

Figure 10 *Contaminant distributions in Case 3*

Arranging a Table-Type Obstacle (Case 4)

The flow and diffusion fields for Case 4, where a table-type obstacle is placed in contact with the side wall, are illustrated in Figures 11 and 12.

Velocity Field A large recirculating flow appears above the obstacle (Figure 11a). The airflow pattern on the top face is shown in Figure 11c. The air under the top face moves along the side wall and toward the exhaust opening (Figures 11b and 11d). The flow pattern in the open area on the right side is the same as in Case 0 where no obstacle is placed (Figure 11a). Thus the area affected by the obstacle is rather small and is confined within the area around the table.

Contaminant Diffusion Field When the contaminant is generated on the top face of the table (Point A), the region from the floor to the ceiling is highly contaminated (Figures 12a and 12b). But the contaminated area is limited to the left third of the room. The value of SVE1 in this case is 1.4, much smaller than in Case 1 (2.1). Hence, it is much more efficient to exhaust

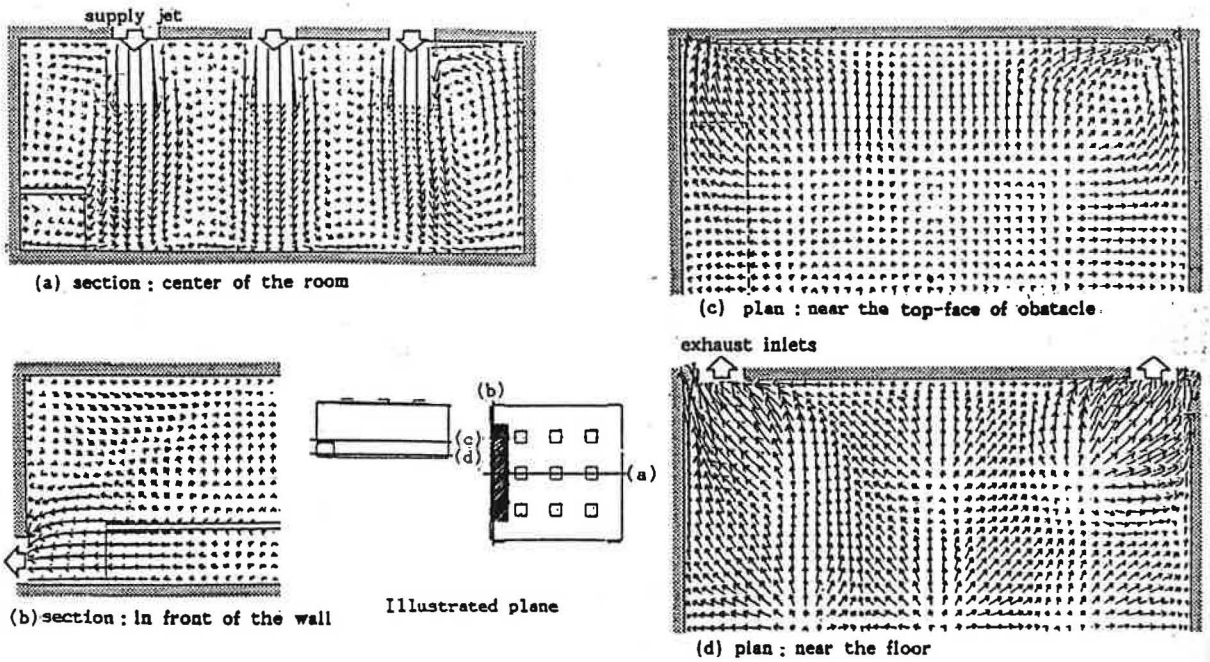

Figure 11 *Velocity vectors in Case 4*

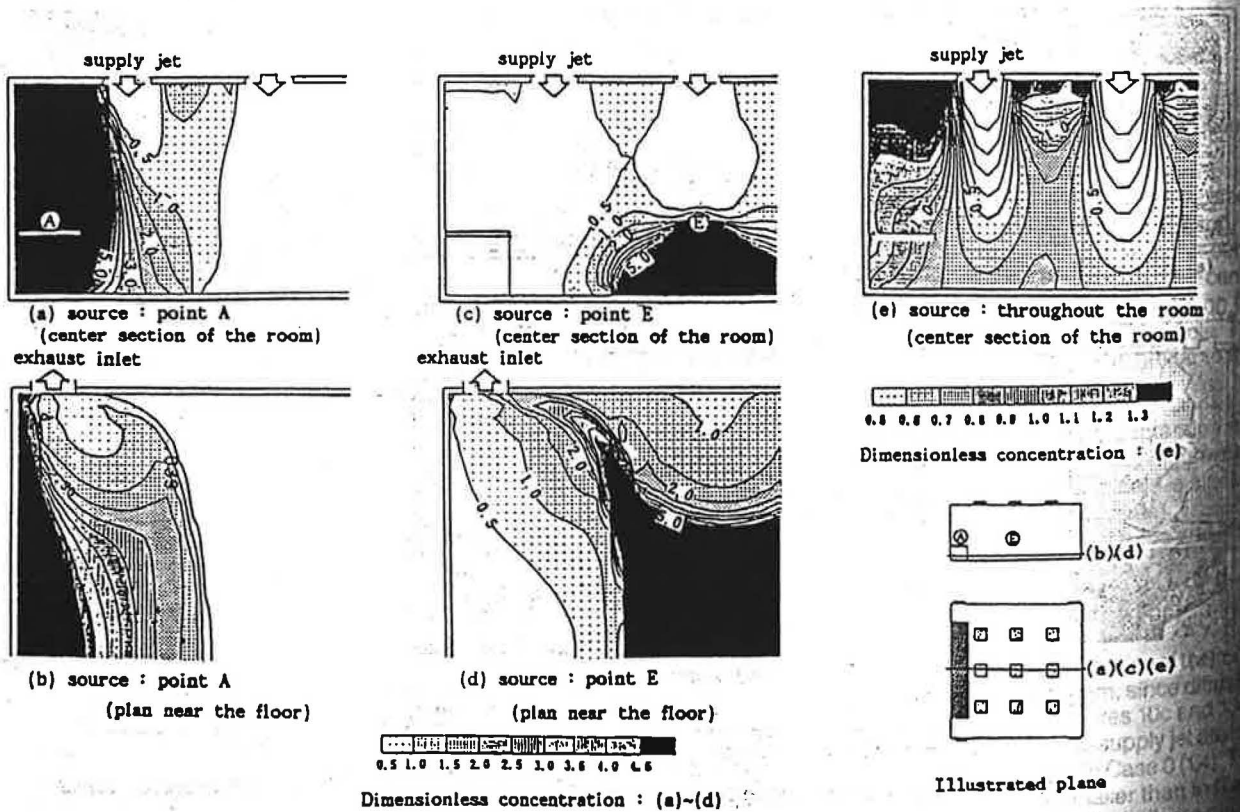

Figure 12 *Contaminant distributions in Case 4*

contaminant with a table-type obstacle than with a box-type obstacle. The value of SVE2 in this case is 2.5, the same as in Case 1.

When the contaminant is generated at the center of the room (Point E), it spreads around the center near the floor (Figures 12c and 12d). The air around the table is very clean, since the three supply jets along the side wall attack the table. The value of SVE1 is 1.3, considerably smaller than in Case 1 (1.6). It can thus be concluded that a table-type obstacle is superior to a box-type obstacle from the viewpoint of ventilation efficiency. The value of SVE2 is 4.2, the same as in Case 1.

The value of SVE3 (Figure 12e) is high in the area above the obstacle, particularly near the ceiling, but it is smaller than in Case 1 (Figure 4e).

INFLUENCE OF LOCATION OF MANY OBSTACLES WITHIN THE WHOLE SPACE (Case 5)

In real clean rooms, many obstacles are usually present. In Case 5, three box-type obstacles are placed beside the walls and in the center of the room (see Figure 1). The flow and diffusion fields in Case 5 are shown in Figures 13 and 14.

Velocity Field

The flow pattern on the top face of the obstacle is shown in Figure 13c. The horizontal flow on the top face of the wall-side obstacle is directed mainly toward the exhaust opening. The supply jets attack the top face of the centered obstacle, thereby causing the airflow to diverge in all directions. Recirculating flows appear in front of the front and back faces of the obstacles (Figure 13a). The resulting flow field in Case 5 may be interpreted as a combination of the flow field of Case 1 (one wall-side obstacle) and Case 2 (one centered obstacle).

Contaminant Diffusion Field

Point Generation of Contaminant When the contaminant is generated on the top face of the wall-side obstacle (Point A, Figure 14a), the contaminant spreads into half the room. The area around the wall-side obstacle is highly contaminated. The value of SVE1 is 2.6, much larger than in Cases 0, 1, and 4. The value of SEV2 is 3.0, similar to Case 0.

When the contaminant is generated at a position between the obstacles (Point C, Figure 14b), the contaminant spreads into half the room. A highly contaminated area appears at the recirculating region in front of the back face of the centered obstacle. The value of SVE1 is 1.5, a little larger than in Case 0 (1.4). The value of SVE2 is 4.0, also larger than in Case 0 (3.4).

When the contaminant is generated at the top face of the centered obstacle (Point E, Figure 14c), the whole area of the room is contaminated except for around the supply jet. A highly contaminated area appears at the recirculating region in front of the front and back faces of the centered obstacle. The value of SVE1 is 2.0, much larger than in Cases 0 through 4.

Uniform Generation of Contaminant on a Surface When the contaminant is generated uniformly on the top surface of the centered obstacle (Figure 14d), it spreads into the whole space of the room except for around the supply jet. In this type of generation, the highly contaminated area is limited to a thin layer above the contaminant-generating surface.

When the contaminant is generated uniformly on the floor between the obstacles (Figure 14e), it also stays in a thin layer above the contaminant-generating floor and in the recirculating region in front of the front and back faces of the centered obstacle. In this type of contaminant generation, air on the top faces of the obstacles remains very clean.

The value of SVE3 (Figure 14f) is higher near the ceiling and at the recirculating region in front of the front and back faces of the obstacles.

COMPARISON OF CONTAMINANT DIFFUSION FIELDS BY MEANS OF SVE1, 2, AND 3

Study Based on SVE1

The values of SVE1 for all cases and for all contaminant generation points are given as the upper line in each space in Table 4. SVE1 shows a larger value when the contaminant is generated near the wall. It increases when the number of obstacles is increased.

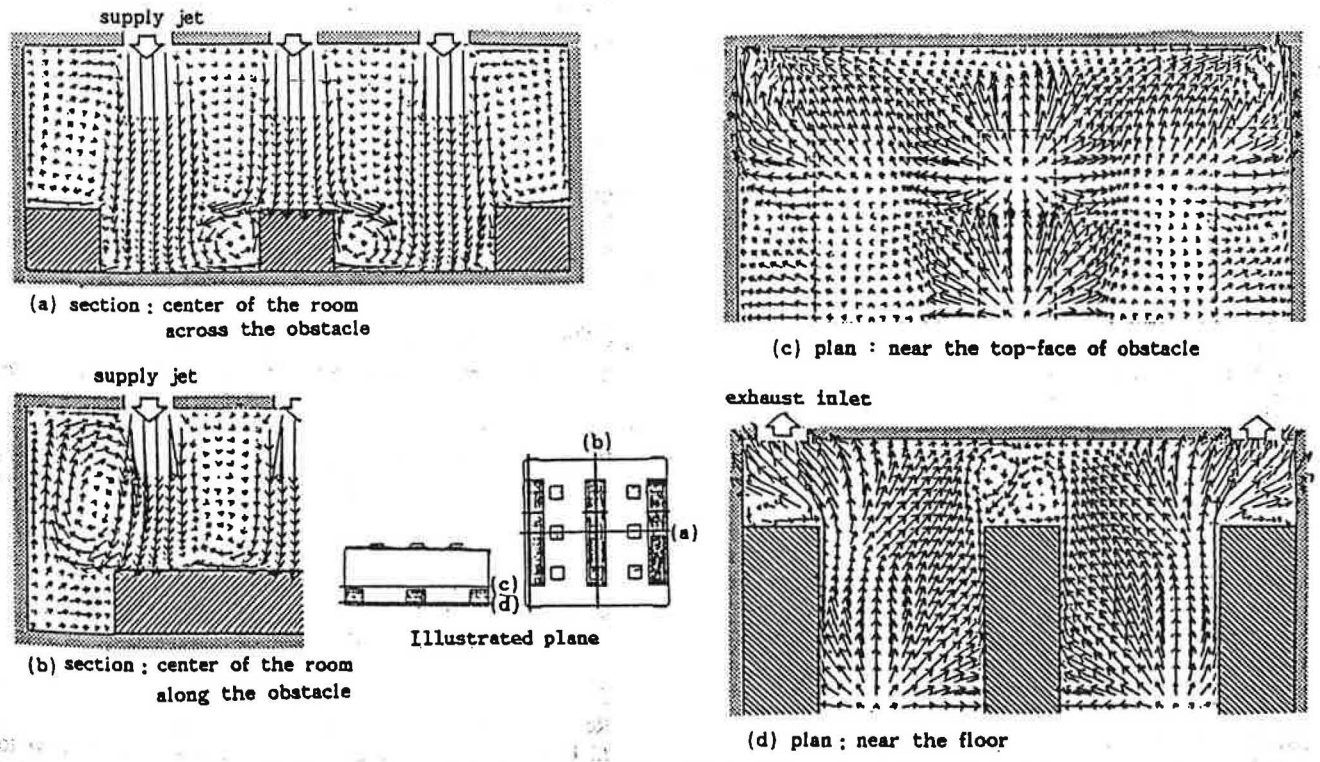

(Case 5 : three box-type obstacles are placed in contact with the walls and in center of the room)

Figure 13 *Velocity vectors in Case 5*

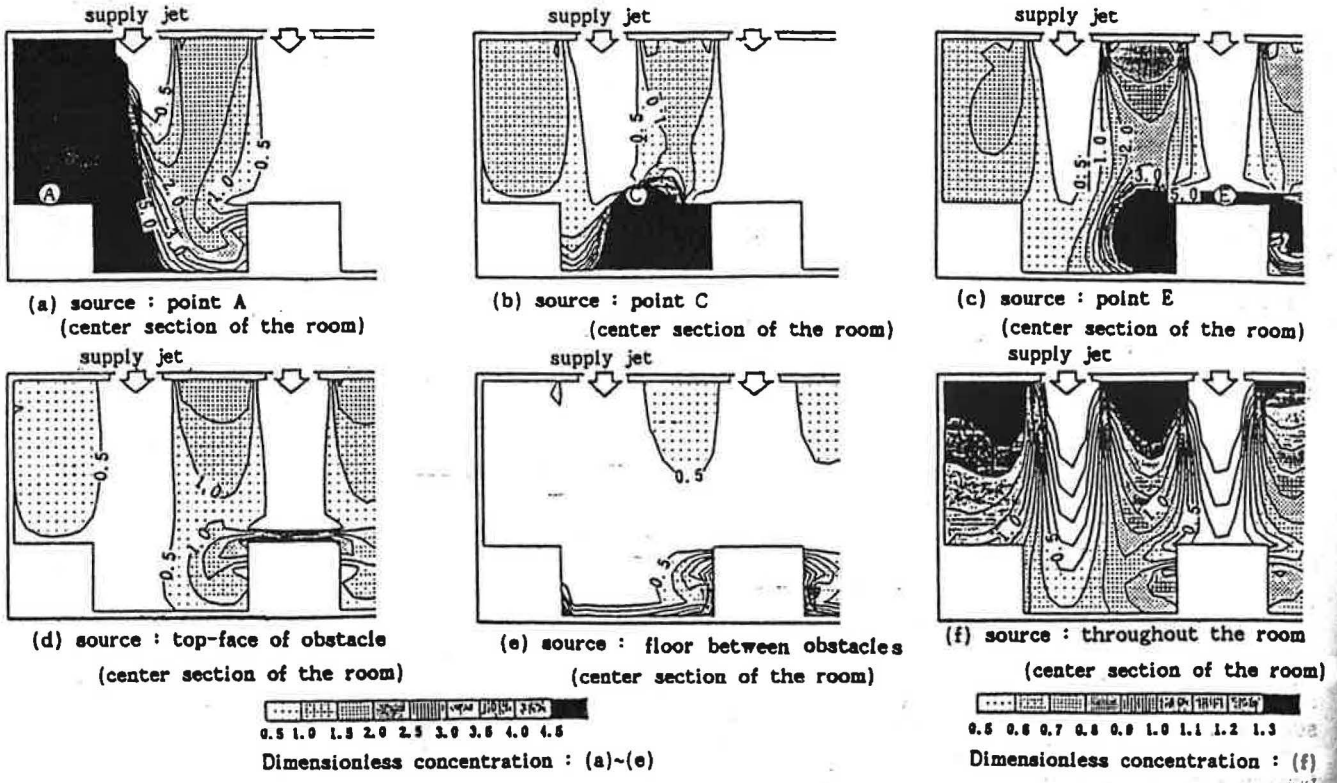

Figure 14 *Contaminant distributions in Case 5*

Study Based on SVE2

The values of SVE2 are tabulated as the lower line in each space in Table 4. SVE2 shows a smaller value when the contaminant is generated near the wall. It increases as the source point moves toward the center of the room. The value of SVE2 is not influenced as much by the position of the flow obstacle.

Study Based on SVE3

A high value for SVE3 appears near the ceiling for all cases. When a recirculating flow forms around the obstacle, SVE3 becomes higher in that region. The supplied clean air takes longer to reach these areas, so there is a much greater possibility that the air in this region will be contaminated.

CONCLUSIONS

The effects of various flow obstacles on the flow and diffusion fields in a conventional-flow-type clean room have been analyzed by means of numerical simulations. The results are as follows:

1. The numerical simulation of flow and diffusion fields with obstacles corresponds rather well to model experiments. The velocity deviations between simulation values and observed ones remain below 5% for almost the whole room space. The contaminant concentration deviation ranges below 10% to 20% for almost the whole space.
2. The effect of the placement of an obstacle on the flow field is usually confined within the space around the obstacle, but the flow field within the "flow unit" in which the obstacle exists is influenced greatly.
3. The placement of a flow obstacle makes the flow field around it very complicated. Consequently, the process of exhausting the contaminant becomes complicated, and the concentration of the contaminant in the recirculating flow region usually becomes higher.
4. Even if the effect of the placement of an obstacle on the velocity field seems to be small, the contaminant diffusion field is often influenced greatly by the arrangement of a flow obstacle.
5. The placement of an apparatus should be selected with the properties of the diffusion field in mind in order to take advantage of the flow structure of the conventional-flow-type clean room.
6. The table-type flow obstacle is generally superior to the box-type flow obstacle from the viewpoint of ventilation efficiency.
7. The SVEs are very useful measures for analyzing the diffusion field and also very strong tools for estimating the ventilation efficiency.

ACKNOWLEDGMENT

The authers are grateful for the assistance of Y. Takahashi and T. Kitazawa, members of the principal author's laboratory. This study has been partially supported by a grant-in-aid for scientific research from the Japan Ministry of Education, Culture and Science.

NOMENCLATURE

C_0	= representative concentration for nondimensionalization defined by mean concentration at exhaust opening
C_μ, C_1, C_2, C_3	= empirical constants in k-ϵ turbulence model
E	= empirical constant in log law, 9.0 in case of smooth wall
k	= turbulence kinetic energy
ℓ	= length scale of turbulence
L_o	= representative length for nondimensionalization defined by width of supply outlet (0.6 m; see Figure 1)
P	= mean pressure
Re	= Reynolds number = U_oL_o/ν
U, V, W	= X, Y, Z components of mean velocity vector
u, v, w	= fluctuating components of velocity vector
U_i, U_j	= components of mean velocity vector

U_o = representative velocity for nondimensionalization defined by supply jet velocity (1.0 m/s; see Figure 1)
ϵ = turbulence dissipation rate
κ = von Karman constant, 0.4
ρ = fluid density
ν = molecular kinematic viscosity
ν_T = eddy kinematic viscosity
$\sigma_1, \sigma_2, \sigma_3$ = turbulence Prandtl/Schmidt number of κ, ϵ, C (see Table 2)

REFERENCES

Kato, S., and S. Murakami. 1988. "New ventilation efficiency scales based on spatial distribution of contaminant concentration aided by numerical simulation." *ASHRAE Transactions*, Vol. 94, Part 2, pp. 309-330.

Launder, B.E., and D.B. Spalding. 1974. "The numerical computation of turbulent flows." *Computer Methods in Applied Mechanics and Engineering*, Vol. 3, pp. 269-289.

Murakami, S., and H. Komine. 1980. "Measurement of three components of turbulent flow with tandem hot-wire probe." *Transactions of Architectural Institute of Japan*, No. 297, pp. 59-69.

Murakami, S.; S. Kato; and Y. Suyama. 1987. "Three-dimensional numerical simulation of turbulent airflow in ventilated room by means of a two-equation model." *ASHRAE Transactions*, Vol. 93, Part 2, pp. 621-642.

Murakami, S.; S. Kato; and Y. Suyama. 1988. "Numerical and experimental study on turbulent diffusion fields in conventional flow type clean room." *ASHRAE Transactions*, Vol. 94, Part 2, pp. 469-493.

Murakami, S.; S. Kato; and Y. Suyama. 1989. "Numerical study on diffusion field as affected by arrangement of supply and exhaust openings in conventional flow type clean room." *ASHRAE Transactions*, Vol. 95, Part 2.

Viecelli, J.A. 1971. "A computing method for incompressible flows bounded by moving walls." *Journal of Computational Physics*, Vol. 8, pp. 119-143.